microstrip parallel-coupled filters. For example in [17], instead of the microstrip open ends in the traditional parallel-coupled filter, there are microstrip gaps in the modified filter and these gaps are of the offset type. By carefully choosing the gap width, one can optimize the stopband rejection and the response symmetry. This method lacks in prescribing straight forward design procedure and is rather iterative. The method proposed in [18] extends the odd mode phase length by allowing the coupled lines to overlap lines outside the resonator. This configuration makes the odd mode length longer than the even mode and thus compensates for the phase velocity difference between the two modes. However, this method significantly increases the filter bandwidth because the coupling of each resonator is increased. Further, according to this design given in [19], the attenuation poles can be obtained at any desired frequency by means of coupling structures. Thus, a filter with excellent attenuation characteristics for various applications can be achieved. However, due to the anti-parallel coupling structure in the design, the filter occupies much larger space and thus not suitable for the application where space is primary constraint. Lately, another interesting method is presented in [20] to suppress the first spurious response of microstrip parallel-coupled filters. Grooves in the substrate are oriented parallel to all coupled lines and just next to them. It is shown that the grooves equalize the even- and odd-mode phase velocities in microstrip coupled lines and, thus suppress the spurious response. The two grooves with proper width and depth are cut along the microstrip coupled lines and just beside them. However, cutting grooves adds extra machining work and the effectiveness of this method may vary from substrate to substrate which have different compositions.

The design of a stripline parallel-coupled BPF with improved upper sideband rejection slope is reported in [21]. In this work, the same concept is adopted to realize parallel-coupled BPF on microstrip. It is well known that in stripline, the conductor is embedded in a homogeneous and isotropic dielectric, and the phase velocity and the characteristic impedance of the dominant mode TEM do not vary with frequency. In the proposed design, each pair of the coupled lines has one section lengthened by an offset δ, while the adjacent section is shortened by the same amount. By introducing such offsets (δ), the transmission line between each J-inverter is preserved as a λ/2 transmission line resonator. The transmission zero between the fundamental and 1st harmonic can be shifted and controlled by the amount of δ offset. By shifting the transmission zero close to the center frequency of the filter, higher rejection at the desired frequency could be achieved. However, there is one constraint in the design. In order to preserve the half-wavelength resonators in the parallel-couple filters, this design can only be applied to even order filters. In the modified filter, the transmission zeros occur at the frequency for which the physical lengths of the 90^0+ δ sections correspond to a half-wavelength where δ is the offset length. This can be written as:

$$L\left(90^o+\delta\right)_{f_o} = L\left(180^o\right)_{f_1} \quad (4)$$

where f_1 the new frequency at which transmission zero occurs.

In our design, the center frequency is 8 GHz. The third harmonic of the active multiplier lies at 12 GHz. It is computed from expression (4) that for $\delta=30^0$, the transmission zero occurs at 12 GHz and results maximum attenuation. Once the offset length is determined, the rest of the design steps are as follows. The element values of a 4th order Chebyshev response filter with 0.01 dB ripple are calculated. The J-Inverter values for the filters are calculated using expressions (5-6). Then, the corresponding even and odd mode impedances for the filters with $\delta=0^0$ and $\delta=30^0$ have been computed using expressions (7-8). The computed even and odd mode impedances are given in Table 2. A LineCalc tool from Agilent is used to calculate the physical dimensions of the microstrip coupled lines for the two filters. It may be noted that for the Stripline coupled filter design, the circuits with desired passband responses can be exactly synthesized. The values of even-mode impedance, odd-mode impedance, and electrical length for each coupled-line section could be well determined. However, if the same design is realized on microstrip, the values of electrical length are different for even and odd modes [22]. Due to this difference, we have experienced degraded performance of filters in terms of increased reflection, passband variations and relatively higher insertion loss both in simulations as well as in measured results. The layout of the two filters is shown in Fig. 6. The two filters with 0 and 300 offset have been fabricated and tested. The measured versus simulated results of each filter are shown in Fig. 7 and Fig.8. The measured results of two fabricated filters are illustrated in Fig.9 and the measured performance is compared in Table 3. The modified BPF with 30^0 offset exhibits and improved upper sideband suppression of 16.5 dB when compared with the conventional design with 0^0 offset.

$$\frac{J_{01}}{Y_0} = \sqrt{\frac{\pi}{2}\frac{FBW}{g_0 g_1}} \quad (5)$$

$$\frac{J_{j,j+1}}{Y_0} = \frac{\pi FBW}{2}\frac{1}{\sqrt{g_j g_{j+1}}} \quad (6)$$

where j= 1 to n-1

$$Z_{0o} = \left(\frac{1}{Y_0}\right)\frac{1-\left(\frac{J}{Y_0}\right)Co\sec\theta_c+\left(\frac{J}{Y_0}\right)^2}{1-\left(\frac{J}{Y_0}\right)^2 Cot^2\theta_c} \quad (7)$$

$$Z_{0e} = \left(\frac{1}{Y_0}\right)\frac{1+\left(\frac{J}{Y_0}\right)Co\sec\theta_c+\left(\frac{J}{Y_0}\right)^2}{1-\left(\frac{J}{Y_0}\right)^2 Cot^2\theta_c} \quad (8)$$

Table 2: Even and odd mode impedances of 0 and 30^0 offset.

Offset (δ) deg	$Z_{01e}=Z_{45e}$	$Z_{01o}=Z_{45o}$	$Z_{12e}=Z_{34e}$	$Z_{12o}=Z_{34o}$	Z_{3e}	Z_{3o}
0	84.5	37.5	60	43	57	44.5
30	91.3	36.9	61.2	42.3	57.9	44

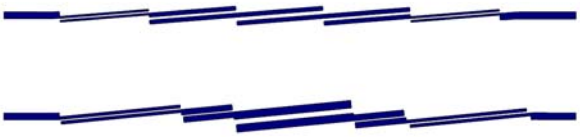

Fig. 6 Layout of (top) conventional BPF with δ=0^0 (bottom) modified BPF with δ=30^0

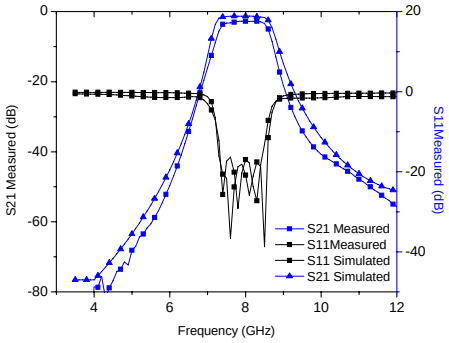

Fig. 7 Simulated and measured response of conventional (δ=0) BPF.

Table 3: Measured results of conventional and modified BPF.

Parameters	***Conventional***	***Modified***
Center frequency (GHz)	8	8
Bandwidth (GHz)	1.35	1.4
Insertion loss (dB)	2.7	3.0
Rejection at 5 GHz	-80	80
Rejection at 12 GHz	-55.5	-72

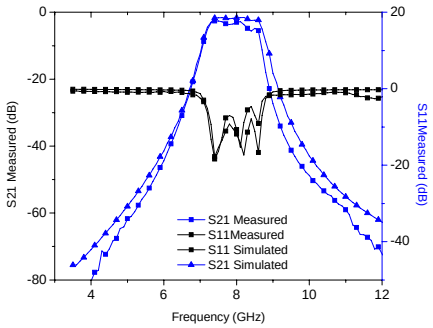

Fig. 8 Simulated and measured response of modified (δ=30^0) BPF.

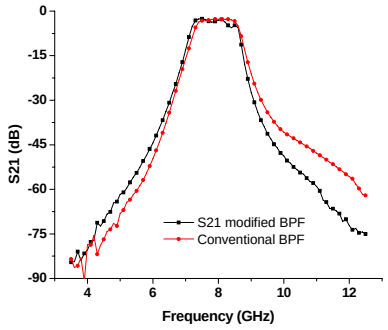

Fig. 9 Comparison of conventional and modified BPFs.

3.4 Notch filter design

The 4 GHz input signal from the synthesizer unit contains 23 dBc half frequency spur. In order to obtain spurious free output spectrum of the front-end receiver, this 2 GHz harmonic needs to be suppressed. A microstrip notch filter with three open-circuited stubs for a FBW = 0.5, centered at 2 GHz frequency is designed. The shunt quarter wavelength open-circuited stubs are separated by unit elements. The unit element is again λ g/4 long at the center stop band frequency [23]. The characteristic impedances for the open-circuited stubs and unit elements are calculated for the desired specifications. The λ g/4 comes out to be 19 mm long and such dimensions could not be accommodated in the available space. One of the options is to realize the filter on a different substrate with a much higher dielectric constant such as 10.8. In order to realize the filter on the same substrate, a meander line structure is adopted as depicted in Fig.10. This scheme significantly reduces the filter size. However, the discontinuities and the coupling effect needs to be considered. The open-end, T-junction and bend effects

have been taken into account to determine the final filter layout. The design is optimized for improved performance with a steeper stopband response. The measured results show the suppression at 2 GHz is more than 55 dB as shown in Fig.11.

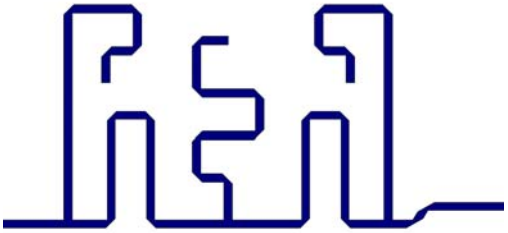

Fig. 10 Meandered line notch filter layout.

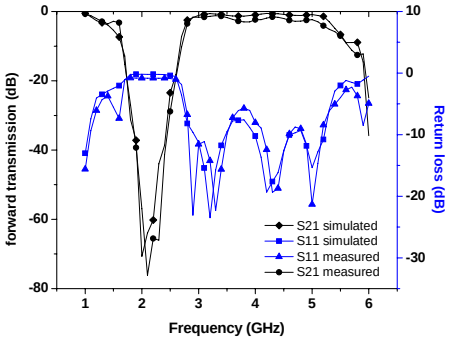

Fig. 11 Meandered line notch filter simulated and measured results.

4. Front-end measurements

The die chips are eutactically attached with the metallic enclosure surface. The bond wire lengths are kept as short as possible. The two front-end receivers are measured on Agilent PNA N5225A. Fig.12 and 13 shows the four fabricated front-end receivers and measurement setup respectively. The measured gain and frequency response of the two receivers along with the simulated one is depicted in Fig.14. The measured gain is 40 dB in the working band of 33-35 GHz. The image rejection is better than 40 dB. The gain and frequency response of the two receivers are in good match. The spectral analysis of the front-end exhibits good spurious free passband spectrum as depicted in Fig.15. The measured noise figure of the two receivers is 4.0 dB and 4.15 dB respectively and are in good agreement with the theoretical one. The breakdown of the theoretical noise figure along with the measured results is given in Table 4.

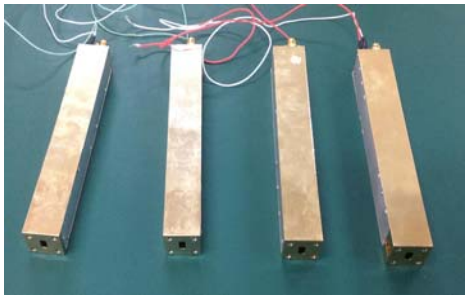

Fig. 12 Fabricated front-end receivers.

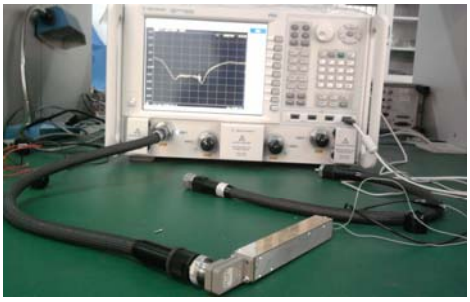

Fig. 13 Measurement setup.

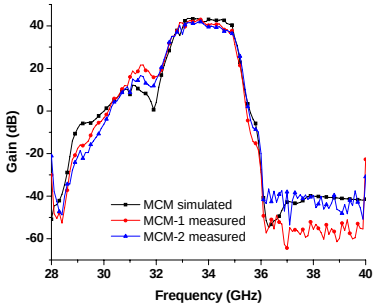

Fig. 14 Measured frequency response of two front-end receivers

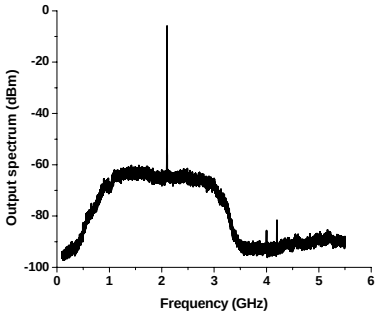

Fig. 15 0.1 GHz-5.5 GHz output spectrum the front-end

Table 4. Comparison of theoretical and measured noise figure

Parameters	*Theoretical*	*Measured)*
LNA noise figure (dB)	2.7	4.10
Waveguide-to-microstrip transition loss (dB)	0.7	
50 ohms matched line loss (dB)	0.2	
Total noise figure according to Friis expression (dB)	4.0	

In order to validate the performance of the front-end receivers for imaging applications, a preliminary test setup is established to compute the correlation coefficients. The setup comprises of a matched noise source, variable attenuator, variable phase shifter, two fabricated MMW front-end receivers, IF IQ (In phase- quadrature) receivers and DSP unit. The system level test setup is depicted in Fig.16 (IF IQ receiver and DSP unit not shown). A power divider feeds the noise signal to the two font-end receivers. A variable phase shifter which follows the power divider is introduced in one the receiver path to obtain different correlation coefficients. The IF IQ receiver translates the 2 GHz output signal to 200 MHz IQ baseband signals. Then the baseband signal is sampled in DSP unit and complex correlation coefficients are computed. The correlation coefficient can be tuned by adjusting the phase shifter. Ideally as the phase shifter changes the phase, the real or imaginary part of the complex correlation coefficient should be a cosine curve while in the Cartesian coordinate it corresponds to a circle. Fig.17 illustrates the measurement results which are close to ideal. The gap in the test curve is due to the fact that the phase shifter can only shift the phase up to 280 degrees. Moreover, the circle is not perfect due to the variations in the insertion loss of the phase shifter at different phase angles.

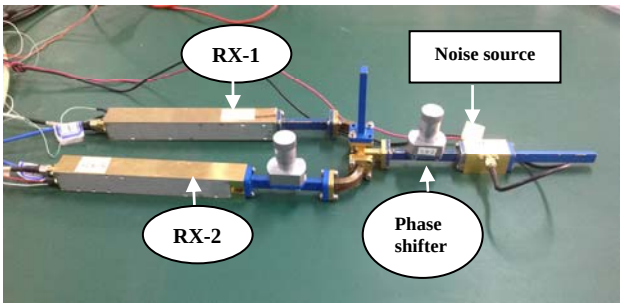

Fig. 16 System level test setup with fabricated two front-end receivers

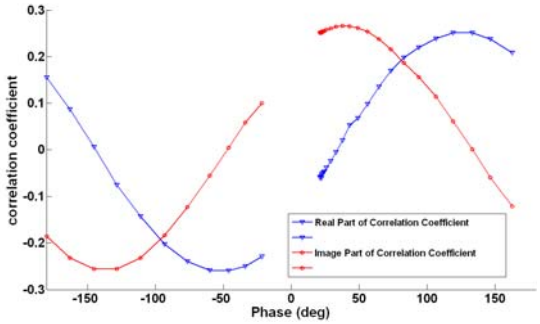

(a)

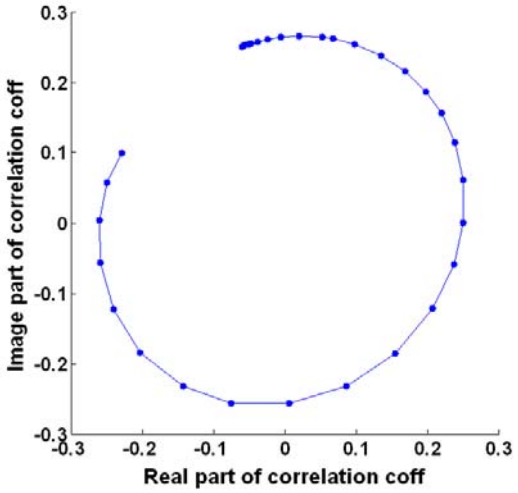

Fig. 17 (a) Complex correlation coefficient cosine curves (b) complex correlation coefficient in the CCS

4. Conclusions

In this paper, a highly integrated Ka band front-end receiver module for a passive Ka band imager is designed, fabricated and tested. All the blocks of the receiver operating from 2 GHz to 34 GHz are realized on a single, low-cost soft substrate employing conventional photolithography process. This provides excellent ease of manufacturability and seamless integration. A five-pole all symmetric parallel-coupled BPF is designed to obtain image rejection better than 40 dB. An X band modified parallel-coupled BPF with improved upper sideband suppression is designed and employed for multiplier harmonic suppression. The upper sideband suppression is at least 16 dB better than its conventional counterpart filter. A compact notch filter with a meander line with mitered bends is designed, fabricated and employed in the receiver. The measured gain and noise figure of the front-end is 40 dB and 4.15 dB respectively.

References

[1] Salmon, N. A., P. N. Wilkinson, C. T. Taylor, and M. Benyezzar,"Minimising the costs of next generation aperture synthesis passive millimetre wave imagers," Proc. SPIE, Vol. 8188, 818808, Oct. 6, 2011.
[2] Lovberg, J. A., C. Martin, and V. G. Kolinko, "Video-rate passive millimeter-wave imaging using phased arrays," Proc. MWSYM, 1689-1692, Honolulu, HI, Jun. 3-8, 2007.
[3] Oka, Soichi, et al. "Latest trends in millimeter-wave imaging technology."Progress In Electromagnetics Research Letters 1 (2008): 197-204.
[4] Zheng, Cheng, et al. "A Passive Millimeter-Wave Imager Used for Concealed Weapon Detection." Progress In Electromagnetics Research B 46 (2013): 379-397.
[5] Zheng, Cheng, et al. "Closed Form Calibration of 1bit/2level Correlator Used for Synthetic Aperture Interferometric Radiometer." Progress In Electromagnetics Research M 29 (2013): 193-205.
[6] Skou, Neils. "Microwave radiometer systems: design and analysis." Norwood, MA, Artech House, 1989, 171 p. 1 (1989).
[7] Razavi, Behzad, and Razavi Behzad. RF microelectronics. Vol. 1. New Jersey: Prentice Hall, 1998.
[8] Chen, Jixin, Pinpin Yan, and Wei Hong. "A Ka-band receiver front end module." In Microwave Conference Proceedings (APMC), 2010 Asia-Pacific, pp. 535-537. IEEE, 2010.
[9] Schreiber, Eric, Simon Anger, and Markus Peichl. "Design of an integrated Ka band receiver module for passive microwave imaging systems." In Semiconductor Conference Dresden (SCD), 2011, pp. 1-4. IEEE, 2011.
[10] Delmotte, Peter. "Waveguide-coaxial line transitions." Belgian Microwave Roundtable (2001).
[11] Keam, R. B., and A. G. Williamson. "Broadband design of coaxial line/rectangular waveguide probe transition." Microwaves, Antennas and Propagation, IEE Proceedings. Vol. 141. No. 1. IET, 1994.
[12] Mehdi, Ghulam, Hu Anyong, and Miao Jungang. "A narrowband low noise amplifier for passive imaging systems." In Applied Sciences and Technology (IBCAST), 2013 10th International Bhurban Conference on, pp. 455-458. IEEE, 2013.
[13] Mehdi, Ghulam, Hu Anyong, and Miao Jungang. "Millimetre-wave all symmetric edge-coupled bandpass filter." In Antennas, Propagation & EM Theory (ISAPE), 2012 10th International Symposium on, pp. 1271-1274. IEEE, 2012.
[14] Yang, Baohua, Ghulam Mehdi, Anyong Hu, Yan Xie, Xianxun Yao, Jin Zhang, Cheng Zheng, and Jungang Miao. "The Round-Ended Design and Measurement of All Symmetric Edge-Coupled Bandpass Filter." Progress In Electromagnetics Research C 38 (2013): 191-203.
[15] Riddle, Alfy. "High performance parallel coupled microstrip filters." In Microwave Symposium Digest, 1988., IEEE MTT-S International, pp. 427-430. IEEE, 1988.
[16] Kajfez, D., and S. Govind. "Effect of difference in odd-and even-mode wavelengths on a parallel-coupled bandpass filter." Electronics Letters 11, no. 5 (1975): 117-118.
[17] Chang, C-Y., and Tatsuo Itoh. "A modified parallel-coupled filter structure that improves the upper stopband rejection and response symmetry." Microwave Theory and Techniques, IEEE Transactions on 39, no. 2 (1991): 310-314.
[18] Riddle, Alfy. "High performance parallel coupled microstrip filters." In Microwave Symposium Digest, 1988. IEEE MTT-S International, pp. 427-430. IEEE, 1988.
[19] Matsuo, M., H. Yabuki, and M. Makimoto. "The design of a half-wavelength resonator BPF with attenuation poles at desired frequencies." In Microwave Symposium Digest. 2000 IEEE MTT-S International, vol. 2, pp. 1181-1184. IEEE, 2000.
[20] Moradian, Mahdi, and Majid Tayarani. "Spurious-response suppression in microstrip parallel-coupled bandpass filters by grooved substrates." Microwave Theory and Techniques, IEEE Transactions on 56, no. 7 (2008): 1707-1713.
[21] Soh, Johnson, Siou Teck Chew, and Ban□Leong Ooi. "Parallel-coupled bandpass filter with improved rejection slope using δ□offset length." Microwave and Optical Technology Letters 50.3 (2008): 680-683.
[22] Lee, Hong-Ming, and Chih-Ming Tsai. "Improved coupled-microstrip filter design using effective even-mode and odd-mode characteristic impedances."Microwave Theory and Techniques, IEEE Transactions on 53, no. 9 (2005): 2812-2818.
[23] D. M. Pozar, Microwave Engineering, 2nd ed. New York: Wiley, 1998.

Ghulam Mehdi received his Bachelor of Engineering degree from NED University Karachi, Pakistan and Master of Engineering from Linkoping University, Linkoping, Sweden in 2000 and 2007 respectively. Currently, he is pursuing his PhD degree at Beijing University of Aeronautics and Astronautics University, Beijing, China. His research interest includes microwave and millimeter-wave circuit design.

Hu Anyong received his Bachelor of Engineering degree from the National University of Defence Technology, Changsha, China, in 2003. He got the PhD degree from Beijing University of Aeronautics and Astronautics (BUAA), Beijing, China, in 2009. Currently, he is faculty member at SOE&IE, BUAA, Beijing, China. His research interest includes signal processing, microwave remote sensing and microwave circuit design.

Jungang Miao received the B.S.E.E. degree from the National University of Defence Technology, Changsha, China, in 1982, the M.S.E.E. Degree from Beijing University of Aeronautics and Astronautics (BUAA), Beijing, China, in 1987, and the Dr. rer. nat. Degree in Physics from the University of Bremen, Germany, in 1998. From 1982 to 1984, Dr. Miao was working in Beijing with the Institute of Remote Sensing Instrumentation, Chinese Aerospace, where he developed space-borne micro-wave remote sensing instruments. From 1984 to 1993, he worked at the Electromagnetic Laboratory of BUAA, doing research and teaching in the field of microwave remote sensing. In 1993, he joined Institute of Environmental Physics and Remote Sensing, University of Bremen, Germany, as a staff member doing researches on space-borne microwave radiometry. In October 2003 he returned to the BUAA and since then he has been taking the Chair Professor position at the Electromagnetic Laboratory of BUAA. Dr. Miao's research areas include electromagnetic theory, microwave engineering and microwave remote sensing of the atmosphere, including sensor development, calibration and data analyses.